Int. J. Heat Mass Transfer. Vol. 32, No. 9, pp. 1765–1778, 1989
Printed in Great Britain

0017–9310/89 $3.00 + 0.00

Heat and moisture transfer by natural convection in a rectangular cavity

H. K. WEE,† R. B. KEEY and M. J. CUNNINGHAM‡
Department of Chemical and Process Engineering, University of Canterbury, Christchurch, New Zealand

(*Received* 6 *November* 1987 *and in final form* 22 *February* 1989)

Abstract—The simultaneous transfer of heat and moisture by natural convection in an air-filled cavity of aspect ratio 7.0 is investigated numerically and experimentally for both a horizontal and vertical cavity. The Prandtl number and the Schmidt number used are 0.7 and 0.6, respectively. The finite-difference equations are solved by the dynamic alternating direction implicit (DADI) method. Both aiding and opposing flows are computed for the range of thermal and concentration Grashof numbers which correspond to the actual temperature and concentration gradients found in a typical building cavity in New Zealand ($2 \times 10^5 < Gr_T < 2 \times 10^6$ and $1 \times 10^4 < Gr_C < 2 \times 10^5$). The experimental technique employs two porous plastic plates as the two cavity walls allowing the imposition of simultaneous moisture and temperature gradients. The experimental Nusselt and Sherwood numbers are found to agree well with the theoretical values.

1. INTRODUCTION

COMMONLY in New Zealand, dwellings are constructed with timber-framed walls and ceilings which result in a gap of about 100 mm between the inner lining and the outer cladding. Heat exchange by natural convection between the building and its surroundings is influenced by the configuration and hygrothermal conditions of the cavity. Heating engineers have been concerned with this kind of insulating cavity for a long time [1–6].

The present work was motivated by a need to understand the moisture behaviour of building structures, to provide practitioners with an effective design tool against possible moisture problems, as traditional tools are inadequate for the task [7, 8]. This understanding is being acquired through a programme [3] in which the basic physics of each component of the structure is investigated and these results are then combined into a system-wide model of the structure.

One element of the system is the building cavity. Nusselt numbers for heat transfer across cavities are well known [5], but Sherwood numbers for moisture transfer are not. Indeed, when calculations are required for moisture-transfer rates across building cavities, the Sherwood number is invariably taken as one. The assumption being made is that water vapour is transferred across building cavities through diffusion alone. However, it is clear that buoyant transfer due to air-density differences caused by the spatial distributions of temperature and water vapour concentration will be an important mass transfer mechanism. It is the aim of this work to discover what Sherwood numbers are appropriate for mass transfer in building cavities.

Other issues also bear upon the moisture performance of cavities, particularly exfiltration and infiltration to other regions, both indoors and outdoors. These mechanisms are to be included in any modelling of the moisture performance of the structural system as a whole. Which mechanism dominates depends upon specific details; for example, certain types of structures such as flat roofs with low ventilation are more prone than others to moisture problems, and in this type of structure it is quite likely that buoyant mass transfer across its cavity is the dominant mechanism.

Both experimental and numerical investigations have been carried out for conditions which correspond to the actual temperature and moisture gradients found in a typical building cavity in New Zealand. The governing differential equations of heat transfer are expanded to include the effect of a simultaneous moisture gradient and the resultant equations are solved numerically using a finite-difference scheme. A novel experimental apparatus, which employed two porous plastic plates as the two cavity walls of a simulated building cavity, has been used to validate the results of the numerical predictions.

2. PREVIOUS WORK

Natural convection due to a temperature gradient across the cavity boundaries has been investigated extensively for a range of vertical, horizontal and inclined cavities [1–6]. Excellent reviews on this sub-

† Meat Industry Research Institute of New Zealand, P.O. Box 617, Hamilton, New Zealand.
‡ Building Research Association of New Zealand, Private Bag, Porirua, New Zealand.

NOMENCLATURE

a_i false-transient factor for ith parameter
A aspect ratio [nondimensional]
C relative moisture concentration [nondimensional]
C' moisture concentration [kg m^{-3}]
D moisture-diffusion coefficient in air [m^2 s^{-1}]
g gravitational acceleration [m s^{-2}]
h heat transfer coefficient [W m^{-2} K^{-1}]
H cavity height [m]
k thermal conductivity [W m^{-1} K^{-1}]
L characteristic length (cavity width) [m]
n coordinate distance normal to wall [m]
N buoyancy-force ratio, Gr_C/Gr_T
t relative time, t'^2/L^2
t' time [s]
T relative temperature [nondimensional]
T' temperature [K]
u stream velocity in the x-direction [m s^{-1}]
U non-dimensional stream velocity, vL/ν
v stream velocity in the y-direction [m s^{-1}]
V non-dimensional stream velocity, vL/ν
x relative coordinate distance, x/L
y coordinate distance [m]
Y relative coordinate distance, y/L.

Greek symbols
α thermal diffusivity [m^2 s^{-1}]
β mass transfer coefficient [m s^{-1}]
β_C volumetric coefficient of expansion due to moisture transfer [K^{-1}]
β_T volumetric coefficient of expansion due to heat transfer [K^{-1}]
ζ relative vorticity [nondimensional]
ζ' vorticity [s^{-1}]
ν kinematic viscosity [m^2 s^{-1}]
θ angle of inclination [deg]
φ relative stream function [nondimensional]
φ' stream function [m^2 s^{-1}].

Superscripts
$'$ dimensional quantity.

Subscripts
C moisture transfer case
T heat transfer case
T, C combined heat and moisture transfer
0 receiving surface
1 transferring surface.

Dimensionless groups
Gr_C mass transfer Grashof number, $g\beta_C\Delta CL^3/\nu^2$
Gr_T heat transfer Grashof number, $y\beta_T\Delta TL^3/\nu^2$
Le Lewis number, Sc/Pr
Nu Nusselt number, hL/k
Pr Prandtl number, (ν/α)
Ra_C mass transfer Rayleigh number, Gr_C/Sc
Ra_T heat transfer Rayleigh number, Gr_T/Pr
Sc Schmidt number, ν/D
Sh Sherwood number, $\beta L/D$.

ject have been given by Ostrach [9] and later by Churchill [10]. From these studies the important parameters which govern the convective process within a cavity are the Prandtl number Pr, the aspect ratio A, the Grashof number Gr or the Rayleigh number Ra, and the inclination θ of the cavity with respect to the gravity vector.

From the results of these studies, the rate of heat transfer across the cavity and, to a lesser extent, the flow pattern for a rectangular cavity can be found for cases corresponding to most practical situations.

Comparatively less work has been reported in the literature on free-convective flow in a cavity due to mass gradient or combined heat and mass gradients. The work on convective mass transfer in confined spaces is restricted to the field of electrolysis [7, 11] where the importance of such studies concern the design and operation of electrochemical reactors. The study of simultaneous heat and mass transfer in the field of thermohaline convection, in which the diffusing quantities are heat and salt, is aimed at finding the onset of convective fluid motion and the associated instability phenomena [12, 13]. Such studies will aid in the understanding of layered structures, both in the salinity and temperature, as well as the vertical transport of heat and salt which exist in some parts of the ocean and in salt-water lakes. The behaviour of such layered structures and the stability criteria are thought to have little relevance in an air–water vapour mixture in a building cavity as the Lewis number for a salt solution is typically 300 times larger than the Lewis number for an air–water vapour mixture.

The potential danger of moisture condensation within a building cavity causing wood-rot has long been recognized and studies in this area have been reported [7, 14–16]. These studies are concerned with the interaction of the cavity's moisture behaviour with its surroundings as a whole and do not address the mechanism of moisture transfer within the cavity.

In regard to transport phenomena for convective non-confined flow adjacent to an isolated plate, the earlier works of Mathers *et al.* [17] and Somers [18] yield transport relationships of the form

$$Nu = f(Gr_T + Gr_C(1/Le)^{0.5})$$

and

$$Sh = f(Le^{0.5}, Nu).$$

Their predictions only agree with experimental results for certain ranges of Prandtl number and better agreement is in fact obtained when the Lewis number is omitted from their equations [19, 20]. Gebhart and Pera [21] concluded that the important parameters governing the flow are (i) the Prandtl number; (ii) the Schmidt number; and (iii) the buoyancy-force ratio $N = Gr_C/Gr_T$. They give the effects of the heat and mass gradients on Nusselt number, Sherwood number, temperature field, concentration field and velocity field. The trend of their results is confirmed by the later work of Nilson and Baer [22] and Boura and Gebhart [23], who also gave more information regarding the finer structures of the flow, such as flow reversal beyond the body of the main flow.

Recently, Trevisan and Bejan [24] published the first paper on combined heat and mass transfer study in a tall vertical cavity subjected to uniform heat and mass fluxes along vertical walls. An Oseen-linearized solution is reported for tall spaces with mixtures for $Le = 1$ and similarity solutions for $Le > 1$ in temperature-driven flows and for $Le < 1$ in concentration-driven flows. The analytical solutions were augmented by numerical calculations. As the analytical solutions were confined to $Pr > 1$ and their numerical solutions for $Pr = 0.7$ were not reported for the case of an aspect ratio of 7 and for a buoyancy rate of less than or equal to 1, their results are not directly comparable with those from this work.

3. NUMERICAL FORMULATION

Fluid is contained within a rectangular cavity of aspect ratio $A = H/L$. The third dimension of the cavity is assumed to be large so that a two-dimensional analysis can be applied. Natural convection occurs because of the temperature and/or moisture gradients which exist across the cavity (Fig. 1).

The cavity is defined as a 'vertical cavity' when the angle of inclination θ is zero and a 'horizontal cavity' when $\theta = 90°$. The temperature drop of interest is $\Delta T = T'_1 - T'_0$ and the moisture-concentration change is $\Delta C = C'_1 - C'_0$.

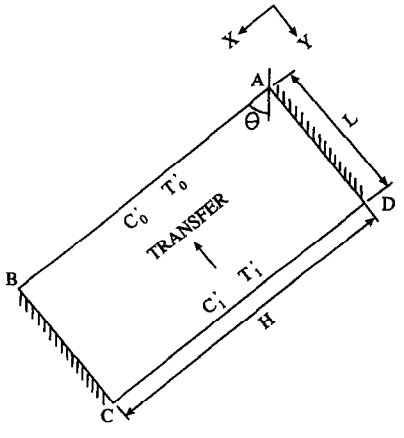

FIG. 1. Cavity configuration and transfer parameters.

For convenience, we define the following non-dimensional parameters:

$$T = \frac{T' - T'_0}{T'_1 - T'_0}, \quad X = \frac{x}{L}, \quad U = \frac{uL}{\nu}$$

$$C = \frac{C' - C'_0}{C'_1 - C'_0}, \quad Y = \frac{y}{L}, \quad V = \frac{vL}{\nu}$$

$$\zeta = \zeta'\left(\frac{L^2}{\nu}\right), \quad \varphi = \frac{\varphi'}{\nu}, \quad t = \frac{t'\nu}{L^2}$$

where the prime indicates the corresponding dimensional quantity.

It is assumed that the buoyancy-generating capabilities of heat and moisture are identical in form, except for the absolute magnitude of the generated buoyancy which is characterized by the magnitude of the respective gradients present. Then the variation in the bulk fluid density causing the motion is a linear function of both ΔT and ΔC. With this formulation, and the inclusion of the false-transient factors of Mallinson and de Vahl Davis [25], the governing dimensionless equations for the conservation of energy, concentration, vorticity and stream function can be written as

$$\frac{1}{a_T}\frac{\partial T}{\partial t} + U\frac{\partial T}{\partial X} + V\frac{\partial T}{\partial Y} = Pr^{-1}\nabla^2 T \tag{1}$$

$$\frac{1}{a_C}\frac{\partial C}{\partial t} + U\frac{\partial C}{\partial X} + V\frac{\partial C}{\partial Y} = Sc^{-1}\nabla^2 C \tag{2}$$

$$\frac{1}{a_\zeta}\frac{\partial \zeta}{\partial t} + U\frac{\partial \zeta}{\partial Y} = \nabla^2\zeta - Gr_T\left(\frac{\partial T}{\partial X}\sin\theta - \frac{\partial T}{\partial Y}\cos\theta\right) - Gr_C\left(\frac{\partial C}{\partial X}\sin\theta - \frac{\partial C}{\partial Y}\cos\theta\right) \tag{3}$$

$$\frac{1}{a_\varphi}\frac{\partial \varphi}{\partial t} = \nabla^2\varphi + \zeta \tag{4}$$

$$U = \frac{\partial \varphi}{\partial Y} \quad \text{where} \quad V = \frac{-\partial \varphi}{\partial X}. \tag{5}$$

The Boussinesq approximation and the assumptions of negligible viscous dissipation and compressibility effects, no internal heat/moisture source or sink being present and the fluid being Newtonian have been used in deriving equations (1)–(5) [20]. This formulation of equations is hybrid between that for natural convection due to temperature difference only and that for heat and mass transfer from a single plate [21, 22]. The boundary conditions used for this work are defined in the following way.

BC1 (at the surface, $Y = 1$)

$$T = C = 1 \quad \text{for cocurrent flow} \tag{6}$$

$$T = 0, C = 1 \tag{7}$$

or

$$T = 1, C = 0 \quad \text{for countercurrent flow.} \tag{8}$$

BC2 (at the surface, $Y = 0$):

$$T = C = 0 \quad \text{for cocurrent flow} \tag{9}$$

$$T = 1, C = 0 \tag{10}$$

or

$$T = 0, C = 1 \quad \text{for countercurrent flow.} \tag{11}$$

BC3 (constant side-wall conditions, at $X = 0$ and A):

$$\frac{\partial T}{\partial X} = \frac{\partial C}{\partial X} = 0. \tag{12}$$

BC4 (zero velocity at the cavity walls, at $X = 0$ and A and $Y = 0$ and 1):

$$U = V = \frac{\partial \varphi}{\partial n} = 0 \tag{13}$$

where the distance n refers to the direction normal to the wall.

The 'dynamic alternating direction implicit' (DADI) method, which was first proposed by Doss and Miller [27], is adopted in this work to solve equations (1)–(5). In this method, the time step for each iteration step is not fixed, but is updated after every iteration to accelerate the convergence to the steady-state solution. This method has been used by Phillips [28] to obtain the solution of natural convection in a square cavity for Rayleigh numbers up to 1×10^6. In this work, numerical results will be presented for a cavity of aspect ratio 7 and for Rayleigh numbers up to 2×10^6. Previously Probert and Dixon [29] have presented numerical results for natural convective heat transfer in a cavity of aspect ratio 5 or greater, but the greatest value of the Grashof number reported was 6×10^5. The results from this work thus extend the range of applicability of the previous numerical simulations.

4. NUMERICAL RESULTS AND DISCUSSION

Computations have been carried out for the following range of parameters:

(i) aspect ratio: 7.0;
(ii) Prandtl number: 0.7;
(iii) Schmidt number: 0.6;
(iv) thermal Grashof number: 1×10^5–2×10^6;
(v) concentration Grashof number: 1×10^4–1×10^5;
(vi) cavity configuration: horizontal and vertical.

Some examples of the results of computations in terms of the dimensionless temperature, concentration and stream-function fields are presented in the next three sections. A complete range of the computed results is given in ref. [20].

4.1. *Temperature, concentration and flow fields in a vertical cavity*

Figure 2 illustrates the streamline and temperature fields for the case of $Gr_T = 2 \times 10^6$, which corresponds to the magnitude of the temperature difference which occurs in a building cavity in New Zealand. It can be seen that secondary cells are well developed and occupy the top and bottom third of the cavity. The results of imposing an additional aiding moisture-vapour pressure gradient which may arise in practice on top of the temperature gradient is illustrated in Fig. 3. (A typical moisture-concentration gradient corresponds to $Gr_C = 8 \times 10^4$.) There are some changes in the secondary and tertiary streamlines at the middle of the cavity, but the form of the primary and the secondary flows at the top and bottom third of the cavity remain essentially the same for both sets of figures. The magnitude of the streamlines is slightly larger for combined heat and moisture transfer (Fig. 3), as is expected from the aiding moisture gradient. The temperature fields of Figs. 2 and 3 do not show a great difference from each other, and in both cases, the grid-spacings used for numerical calculation are

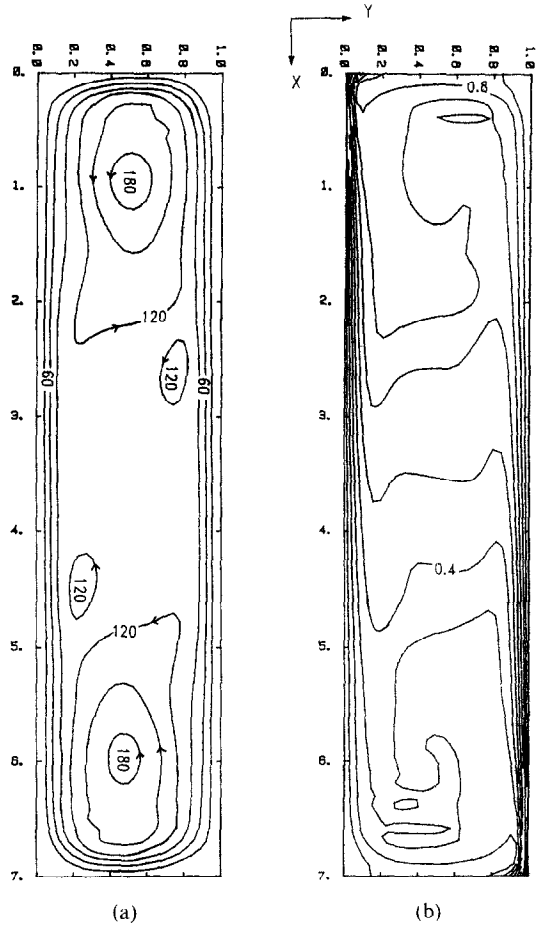

FIG. 2. Streamline and temperature fields for heat transfer in a vertical cavity, $Gr_T = 2 \times 10^6$, $Gr_C = 0$: (a) streamlines; (b) temperatures.

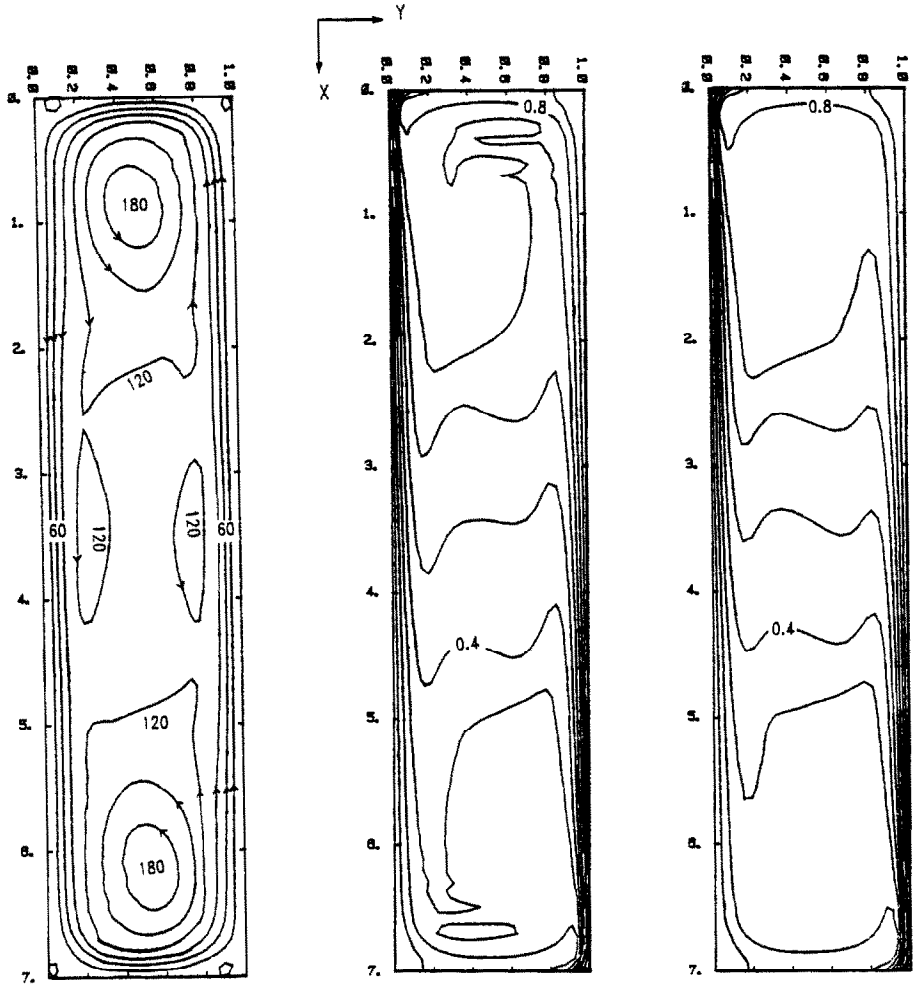

FIG. 3. Streamline, temperature and concentration fields for combined heat and moisture transfer in a vertical cavity, $Gr_T = 2 \times 10^6$, $Gr_C = 8 \times 10^4$: (a) streamlines; (b) temperatures; (c) concentrations.

not fine enough to resolve properly the isotherms of 0.7 and 0.3 near the top and bottom of the cavity where the influence of the recirculating secondary flows is strong.

The effect of a simultaneous temperature gradient on the concentration field can be observed by comparing Figs. 3 and 4. Figure 4 shows streamlines and concentration fields for isothermal mass transfer only at $Gr_C = 1 \times 10^5$, of similar order to Gr_C in Fig. 3. In Fig. 4, the flow field is seen to consist of a series of longitudinal cells (the primary cells). No secondary cells are observed for this case. The concentration field exhibits the usual 'reversal' of contours at the middle and a slight boundary-layer behaviour is developing. The moisture concentration difference across the cavity in Fig. 3 is in fact smaller (by 20%) than that in Fig. 4, yet the presence of the simultaneous temperature gradient in Fig. 3 has generated a stronger convective flow in the cavity than that in Fig. 4.

Figure 5 is an example of the fields resulting from the case of opposing heat and concentration gradients. The concentration gradient is acting from left to right, while the temperature gradient is acting from right to left (as indicated by the magnitude of the respective contours). Note that the convective flow cells are rotating in a clockwise direction, i.e. in the direction caused by the predominant moisture gradient. Both the shape of the temperature and concentration fields are similar to each other regardless of the direction of their respective gradients. If the reverse moisture gradient were absent, the temperature field would be similar to the concentration field in Fig. 4(b), i.e. a mirror image of that in Fig. 5(c).

Although the thermal Grashof number used in Fig. 5 corresponds to an unusually small gradient in practice, the behaviour was found to be similar for higher values of both thermal and concentration Grashof numbers. It illustrates the interdependence of flow, temperature and concentration fields on each other and the importance of the magnitude and the direction

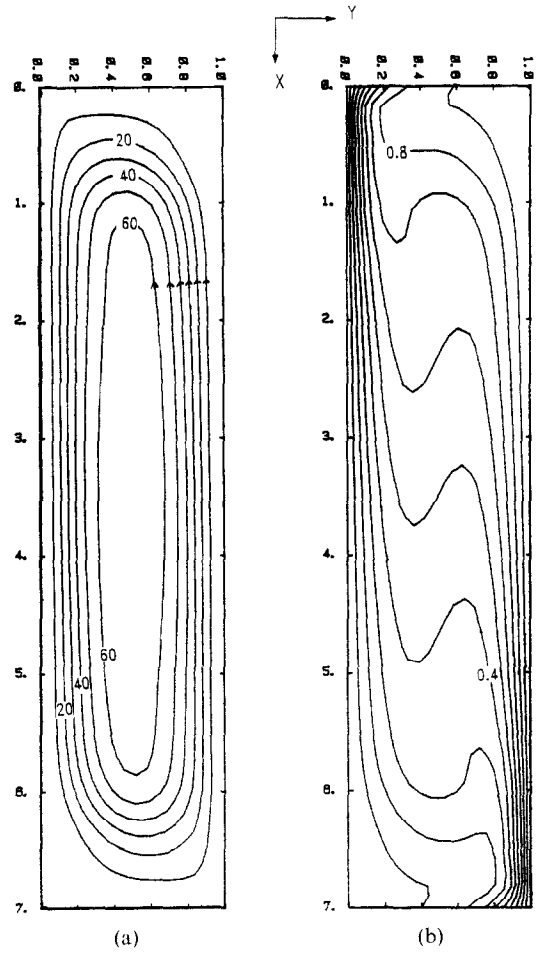

FIG. 4. Streamline and concentration fields for moisture transfer in a vertical cavity, $Gr_T = 0$, $Gr_C = 1 \times 10^5$: (a) streamlines; (b) concentrations.

of the dimensionless driving force (the Grashof number).

4.2. *Temperature, concentration and flow fields in a horizontal cavity*

The flow field in a horizontal cavity with upwards transfer consists of a series of roll cells, each counter-rotating in the opposite direction to its neighbours for all types of boundary conditions. Unlike the vertical cavity, no secondary or tertiary cells are observed on top of the primary cells as the Grashof number is increased. However, the large number of primary cells and their orientation with respect to the physical dimension of the cavity mean that the critical length for numerical calculation lies between the pitch of adjacent counter-rotating cells in the X-direction (see Fig. 1) rather than within the distance of the rotating cells and the walls in the Y-direction, which is for the case of the vertical cavity. This difference in critical length increases the number of grid-points required to produce a solution of comparable accuracy for the horizontal cavity compared with that for the vertical cavity. Perturbation of an initial condition is also needed to start the convective motion.

Figure 6 shows a typical concentration (or temperature) and streamline fields for the case of a small gradient where $Gr_C = 1.41 \times 10^4$. The streamlines consist of eight counter-rotating cells. The concentration field, which consists of parallel horizontal lines when only diffusion is the mode of transfer, is distorted by the convective flow field, with the contours dipping downwards where the flow is going downwards and alternatively rising upwards with the flow.

Figure 7 shows the temperature and stream-function fields for the case $Gr_T = 2 \times 10^6$, which corresponds to the highest dimensionless driving force computed. Again counter-rotating cells are observed, but the number of cells is reduced to seven. The two cells immediately adjacent to the walls are also larger than those in the middle. The flow in Fig. 7 is about 20 times stronger than that in Fig. 6 judging from the maximum values of the respective streamlines. The temperature field is distorted most at the locations where the streamlines were moving up or down, as at a smaller Grashof number, but an almost isothermal region exists at the location corresponding to the centre of each rotating cell.

Figure 8 shows an example for the case of opposing heat and moisture gradients. The moisture gradient is acting downwards, and if it were on its own, it would sustain a transfer process by diffusion only (thus resulting in a series of parallel, horizontal iso-concentration lines in the cavity). However, the presence of the upwards and much stronger simultaneous temperature gradient has resulted in a convective flow being generated and the concentration field is modified to look like the temperature field, as indicated in Figs. 8(a) and (b). Effectively, the mode of moisture transfer from the top to the bottom is now equivalent to a case were the moisture gradient is acting from the bottom to the top, while the rate of moisture transfer is of course significantly increased by the convective process in comparison with the diffusional process alone.

4.3. *Horizontal cavity—downwards transfer*

No convection is observed for the case when the top boundary had a higher potential than the bottom boundary in a cavity. In all cases tried, the perturbation introduced to an initially stable field (diffusion-process dominant) has been unsuccessful in generating any flow and the disturbance disappeared after iteration of the field variables. It is thus concluded that the horizontal cavity with downwards transfer constitutes a stable condition and transfer of heat and moisture is by diffusion only.

5. EXPERIMENTAL APPARATUS

A novel experimental rig was built to test the predictions of Nusselt and Sherwood numbers by the numerical model. Figure 9 illustrates schematically the various compartments of the apparatus and some

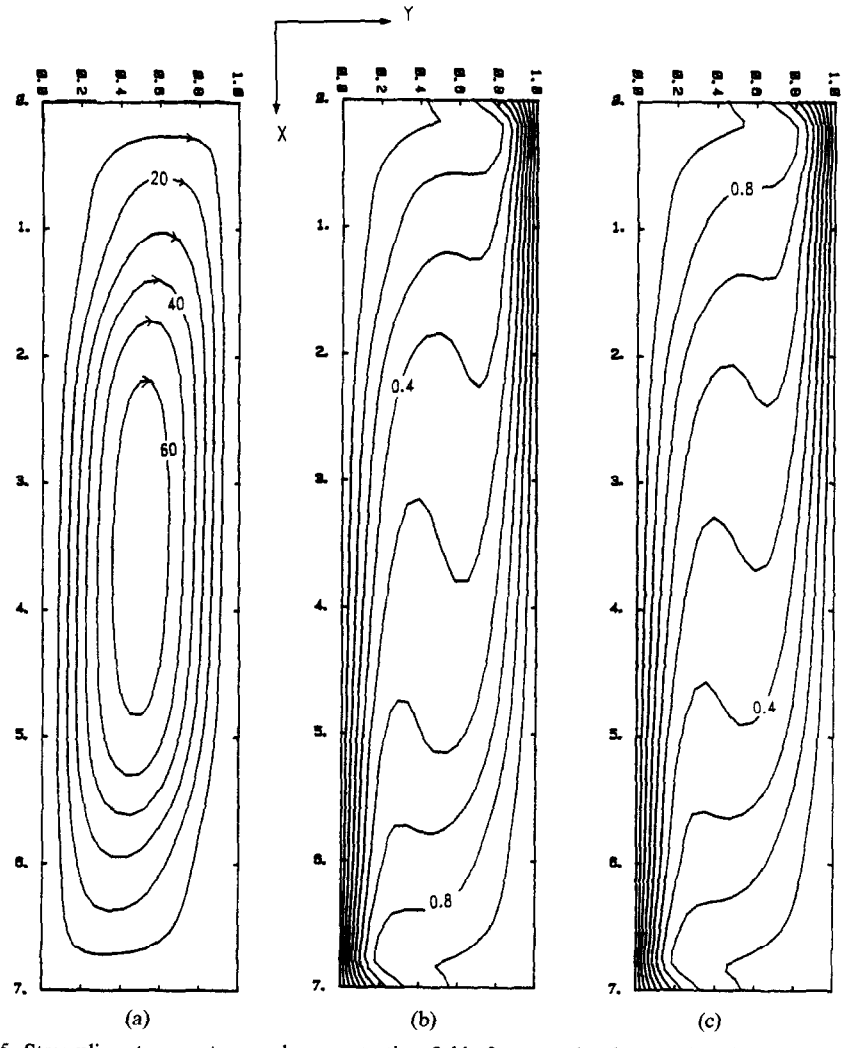

FIG. 5. Streamline, temperature and concentration fields for opposing heat and moisture transfer in a vertical cavity, $Gr_T = 6 \times 10^4$, $Gr_C = -1.2 \times 10^5$: (a) streamlines; (b) temperatures; (c) concentrations.

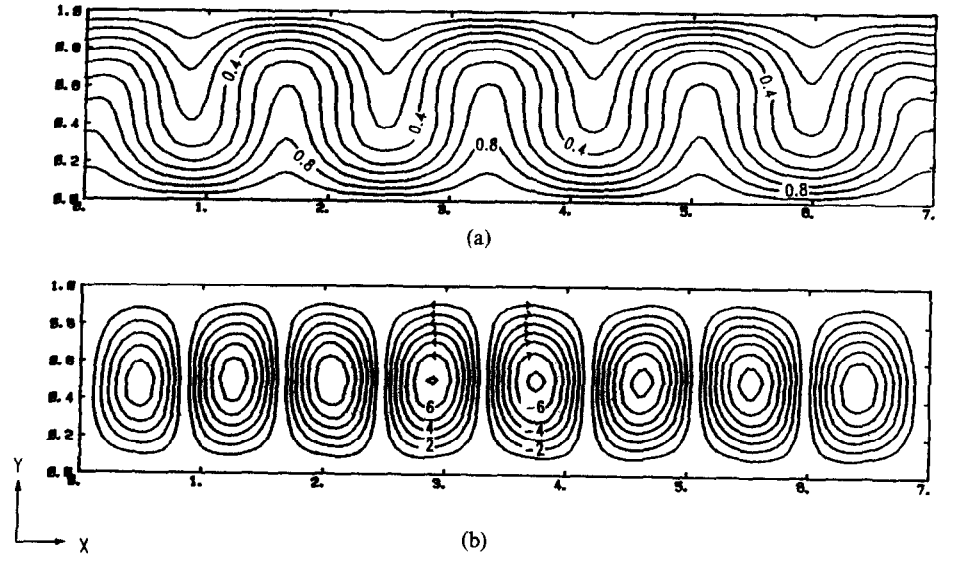

FIG. 6. Streamline and concentration fields for small concentration differences in a horizontal cavity, $Gr_T = 0$, $Gr_C = 1.41 \times 10^4$: (a) concentrations; (b) streamlines (contour level = 1.0).

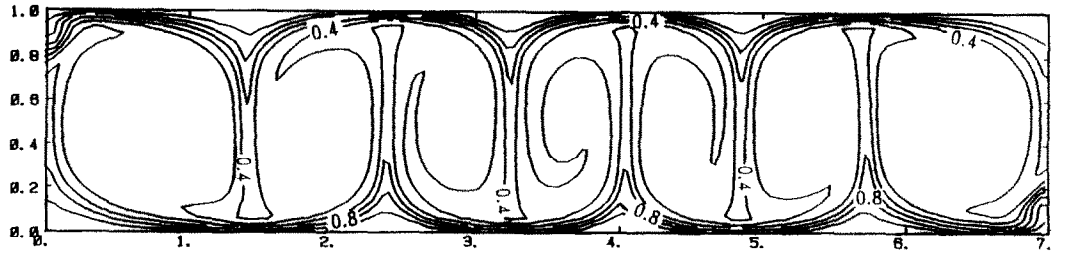

(a)

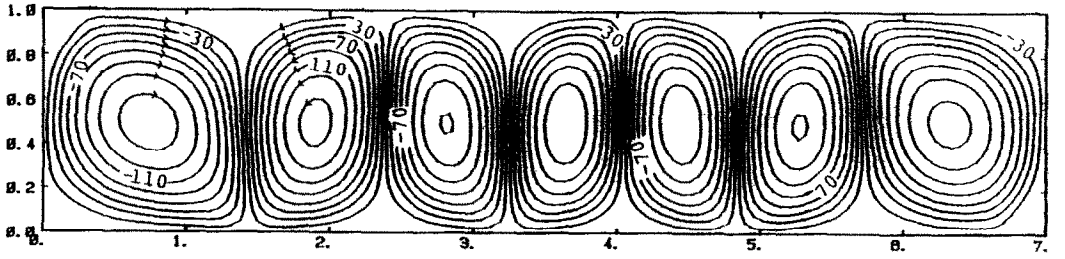

(b)

FIG. 7. Streamline and temperature fields for large temperature difference in a horizontal cavity, $Gr_T = 2 \times 10^6$, $Gr_C = 0$: (a) temperatures; (b) streamlines (contour level = 20.0).

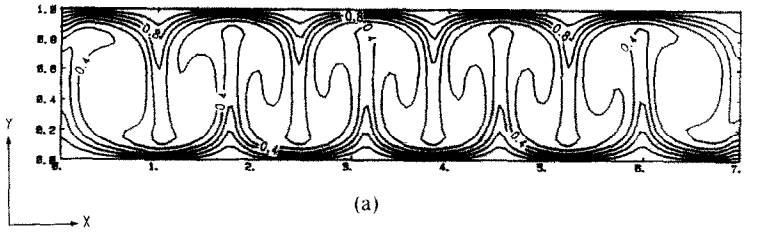

(a)

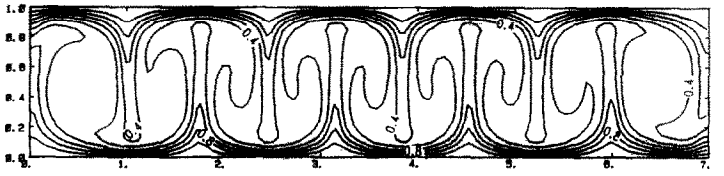

(b)

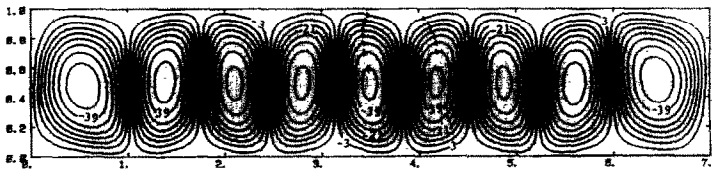

(c)

FIG. 8. Streamline, concentration and temperature fields for opposing heat and moisture transfer in a horizontal cavity, $Gr_T = 5.5 \times 10^5$, $Gr_C = 1.4 \times 10^5$: (a) concentrations; (b) temperatures; (c) streamlines (contour level = 6.0).

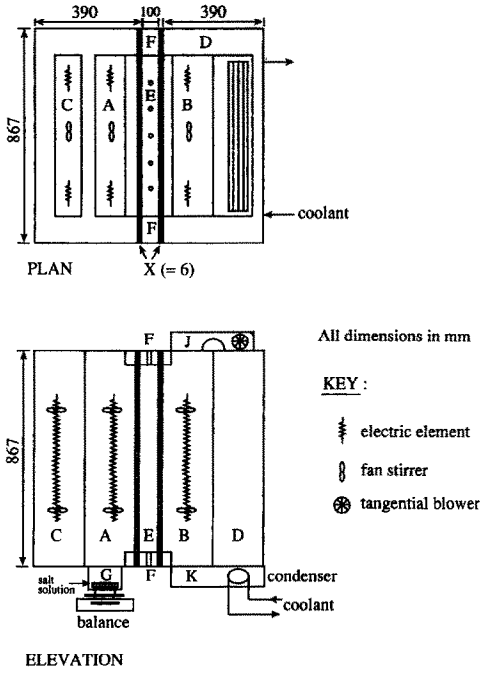

FIG. 9. Schematic diagram of the test equipment in the vertical arrangement.

associated instrumentation. The basic design principle of the guarded box is similar to that given in ASTM C236 [30], with the exception that the moisture-transfer rate is also measured and an air cavity is incorporated.

References [26, 31] give a more detailed description of the experimental apparatus. The apparatus can be arranged either in a 'vertical' position as shown in Fig. 9, or in a 'horizontal' position by tilting the apparatus by 90° and making the necessary changes to the guard chambers G and K. The inert porous sheet is made of high-density polythene particles by a powder-sintering process to yield an average pore size of 200 μm. The thickness of the plate used was 4.75 mm. The whole apparatus was covered with 50 mm thick polystyrene insulating pads which were lined with aluminium foil.

6. THE MEASUREMENT OF HEAT AND MOISTURE-TRANSFER RATE ACROSS THE CAVITY

Consider the case when the controlled chamber A is acting as the source of heat and moisture and the receiving chamber B is acting as the sink. As chambers A and B are controlled to different temperature and moisture levels and separated from the test cavity E by porous boundaries, the boundary conditions across the test cavity should approach that of chamber A on one side, and that of chamber B on the other side. A typical run would take about 8 h to attain the required steady-state thermal and moisture levels in chambers A and B before an experimental run lasting 24 h would begin. The heat input into chamber A was measured by the amount of heat dissipated by the resistive electric heating elements and determined by a power meter which averages the power output of the heater over a certain time period (from 10 s to 8 min), the reading being recorded on a logging computer. By setting chambers A and B to the same temperature above ambient, the heat losses from the rig could be determined.

Four pairs of thermocouples measured the bulk-air temperature in each of the chambers, while six pairs of thermocouples measured the porous plate's surface temperature. To reduce thermal radiation effects, the electric heating elements were specially constructed of polished brass of emissivity 0.03 with a large finned heating area such that the temperature difference between the heater and the bulk air was no greater than 20°C in the worst instance. Radiation shields in the form of perforated aluminium shells protected the bulk air thermocouples. The temperature variation for the bulk-air condition in the well-stirred chambers was typically ± 0.3°C rising to ± 0.5°C for the worst instance, while that on the porous plate surface was typically ± 0.5°C rising to ± 1°C for the worst case. The experimental error for the heat transfer rate across the cavity was typically 13%.

The moisture source was a tray containing a saturated salt solution, which in this case was put in compartment G. The use of various saturated salt solutions enabled the bulk-air relative humidity to be controlled to any desired level in the range of 30–70%. As there is no means to measure explicitly the cavity's moisture boundary conditions on the porous plate surfaces, these conditions were calculated using the porous plate's moisture-resistance value and the Chilton and Colburn analogy [26]. The tray rested on four small tubes which were attached to a plate which rested on a Mettler electronic balance continuously reading and transmitting the weight of the saturated salt solution to a logging parameter. The rate of data logging was once every 4 min for a run lasting about 24 h. The rate of moisture input into the controlled chamber, which was equal to the rate of moisture loss from the tray, was computed by numerical differentiation using the second-order, mid-point method. About 8 h were needed to allow the controlled chamber A to come to steady state before a run could be commenced. The humidity level in each chamber was measured by an EG & G dew-point meter. The dry bulb and the dew-point temperatures would both remain constant to ± 0.3°C during the course of a run. Analogous to the heat transfer rate, the rate of moisture transfer across the cavity was found from the difference between the rate of moisture loss from the tray and the rate of moisture loss from the controlled chamber to the surroundings. The experimental error was typically 1.5% for the moisture-transfer rate across the cavity.

Heat and moisture flows reaching the receiving chamber B were not measured. Both heat and moisture were continuously removed by means of a cooling

coil located in compartment K. The cooling coil also controlled the dew-point temperature of the bulk air in the receiving chamber.

7. THE CHARACTERISTICS OF THE POROUS PLASTIC PLATE

The experimental programme was divided into two categories: those experiments which were performed to determine the characteristics of the porous plates (thermal and moisture-diffusional resistance values, hygroscopicity and thermal emittance); and those experiments which were performed to investigate the simultaneous transfer of heat and moisture across the air-filled cavity. The determination of the characteristics of the porous plastic was necessary for the true boundary conditions of the air cavity to be deduced from known bulk-air conditions. For instance, the boundary condition for moisture transfer in the test cavity can only be deduced from measurement of the bulk-air humidity levels in the controlled and the receiving chambers, since there were no means available which could measure the surface humidity values in the same manner as a thermocouple was able to measure the surface temperature. The characteristic values of the porous plates for both 'vertical' and 'horizontal' cavity arrangements were determined experimentally, and typical values are summarized in Table 1.

The thermal conductivity and the moisture-diffusional resistance values were determined by placing only one porous plate between the controlled and receiving chambers. The boundary conditions across the porous plate and the resultant transfer rate were measured to allow the estimation of the appropriate resistance values. Slightly different values of these transfer parameters were found, according to the orientation, but the differences lie within the uncertainty of the data. The lack of hygroscopicity of the porous plate was found from separate bench-testing at various operating temperatures for the test cavity, while the thermal emittance was determined at 25°C using a Gier–Dunkle infra-red reflectometer.

8. THE CAVITY CASE

8.1. *Heat and moisture transfer in a vertical cavity*

Figures 10 and 11 represent the complete range of experimental Nusselt and Sherwood numbers respectively as a function of the Rayleigh numbers for the 'vertical' cavity. The range of experimental temperature and moisture difference applied across the cavity space corresponds to the level of temperature

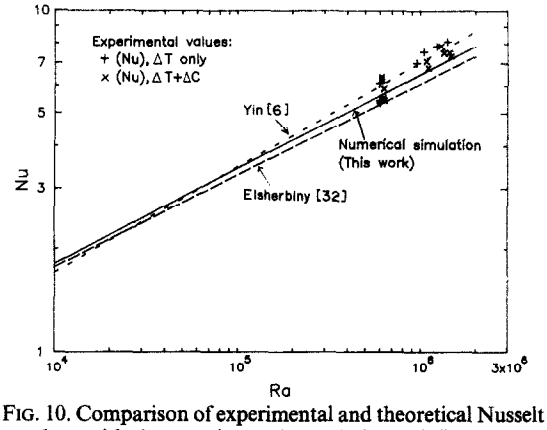

FIG. 10. Comparison of experimental and theoretical Nusselt numbers with the experimental correlations of (i) Yin *et al.* [6] and (ii) Elsherbiny *et al.* [32].

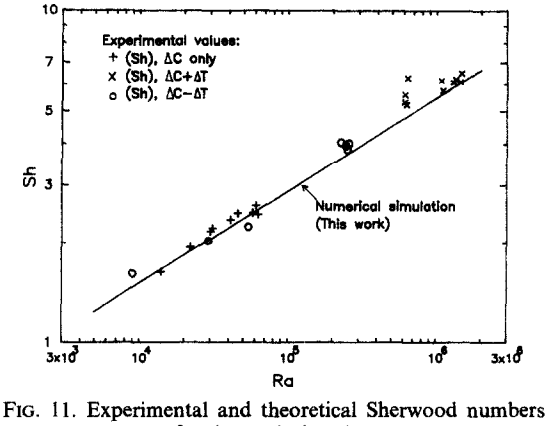

FIG. 11. Experimental and theoretical Sherwood numbers for the vertical cavity.

Table 1. Thermal and moisture-transfer properties of 'Vyon' porous sheet, 200 μm pore size

Parameters	Cavity configuration Vertical	Horizontal
Thermal conductivity for $\Delta T = 6$ K (W m^{-1} K^{-1})	$56 \pm 3 \times 10^{-3}$ (=0.056)	$59 \pm 3 \times 10^{-3}$ (=0.059)
Moisture diffusion resistance for $\Delta P = 533$ Pa (N s g^{-1} m^{-2})	$2.85 \pm 0.11 \times 10^5$	$2.88 \pm 0.11 \times 10^5$
Hygroscopicity	nonhygroscopic	
Thermal emittance:		
smooth side	0.77	0.77
rough side	0.73	0.73

and moisture gradients one would expect to find in a typical New Zealand building. The temperature difference ranged between 6.0 and 16.5 K, with the experimental uncertainty in the Nusselt numbers ranging from ±11 to ±14%, of which two-thirds of the error was due to heat transfer rate measurements and the remaining one-third due to temperature measurements. The vapour pressure used varied from 144 to 747 Pa, with the experimental uncertainty in the Sherwood number ranging from ±16 to ±34%. The uncertainty in determining the boundary values for humidity accounted for about 95% of the error for the Sherwood number.

Figure 10 compares the experimental and theoretical Nusselt numbers for an aspect ratio of 7 from this work with the experimental correlations of Elsherbiny *et al.* [32] and Yin *et al.* [6]. These latter experimental values were obtained from cavities of aspect ratio of 4.9–78.7 and those of Elsherbiny *et al.* from 5 to 110. The numerical results agreed with both sets of published results within experimental uncertainty for the whole range of Rayleigh numbers in Fig. 10 although the correlation of Elsherbiny *et al.* [32] fits the theoretical values better. The numerical results reported in Fig. 10 extend the earlier results of Probert and Dixon [29] for a cavity of aspect ratio 5 or greater, although the agreement with our data for the same range of Rayleigh number is not so good.

The experimental Nusselt number correlation for the vertical cavity shown in Fig. 10 is

$$(Nu) = 0.058[Ra]_{T,C}^{0.346} \quad \text{S.D.} = 0.7 \qquad (14)$$

which agrees with the correlation of Elsherbiny *et al.* [32] and Yin *et al.* [6] within experimental limits of 11–14%. Equation (15) is not recommended for use outside the range of Rayleigh numbers tested.

Irrespective of whether the flow was generated by a pure moisture gradient or a combined heat and moisture gradient, the experimental Sherwood numbers in Fig. 11 can all be characterized by a single correlation found by the least-squares technique

$$(Sh) = 0.113[Ra]_{T,C}^{0.286} \quad \text{S.D.} = 0.3 \qquad (15)$$

where

$$[Ra]_{T,C} = [Ra]_T + [Ra]_C \qquad \text{for cocurrent flow} \qquad (16a)$$

and

$$[Ra]_{T,C} = -[Ra]_T + [Ra]_C \qquad \text{for countercurrent flow.} \qquad (16b)$$

This demonstrated the suitability of the combined Rayleigh number as a measure of the dimensionless driving force. It also supported the postulate that the convecting air has no means of distinguishing between the type of buoyancy that is causing the flow, but merely affected by the magnitude of the buoyancy. Thus, the Sherwood numbers obtained from the case of opposing gradients would always be smaller than the case of aiding gradients for similar values of $[Ra]_T$ and $[Ra]_C$. When compared with the isothermal case, however, the Sherwood numbers for the opposing gradients case can be higher if the temperature gradient is much stronger than the moisture gradient (e.g. for the points at $Ra = 2.5 \times 10^5$ in Fig. 9). Thus, for the case of opposing gradients in the building cavity, the rate of moisture transfer is not governed by moisture-concentration difference but rather by the opposing temperature difference which is principally responsible for generating the convective flow. The direction of the mass transfer is, nevertheless, still from the side of high moisture concentration to the side of low concentration. It is only in an isothermal cavity that the moisture gradients determine both the rate and the direction of moisture transfer.

Figure 11 also compares the experimental Sherwood numbers with the theoretical values from numerical calculation. The agreement between experimental and theoretical values is well within the experimental uncertainty of 16–34%. The good agreement between experimental and theoretical results suggests that the values presented in Fig. 11 are reliable and equation (15) can be used to predict the moisture transfer in a vertical cavity. Alternatively, using the computer model, one can confidently predict the Sherwood number at any Rayleigh number between the limits given in Fig. 11 and more importantly, extend the prediction to other aspect ratios and Rayleigh number ranges where the computer model is expected to hold and where the present apparatus is not capable of producing data without extensive modification, e.g. at Rayleigh numbers less than 10^4. No other results were available from the literature to be compared with the Sherwood numbers in Fig. 11.

The Sherwood numbers for the case of opposing gradients are seen to fall in line with those for the case of aiding gradients in Fig. 11.

8.2. *Heat and moisture transfer in a horizontal cavity*

Figure 12 illustrates the plot of Nusselt and Sherwood numbers against the appropriate Rayleigh number for the case of horizontal cavities with upwards transfer and with downwards transfer. Both aiding and opposing gradients cases were investigated. The range of Rayleigh numbers investigated is similar to those described in Section 8.1. The Nusselt and Sherwood numbers for the case of upwards transfer were 5–9 times the corresponding values for the case of downwards transfer when both the temperature and moisture gradients were acting in the same direction. When the two driving forces are opposing each other, the combined Sherwood number for the case of downwards moisture gradient and upwards temperature gradient lie almost in-line with the concentration Sherwood numbers obtained from the case for upwards isothermal moisture gradient and the combined Sherwood numbers for simultaneous upwards heat and moisture gradients.

8.2.1. *A horizontal cavity with upwards transfer.* As

with the case of the vertical cavity, the dimensionless driving force resulting from the temperature difference was about ten times that generated by the moisture difference for the level of temperature and moisture gradient one would expect to find in an actual building cavity (temperature differences varied from 2.5 to 21 K and moisture vapour-pressure differences from 215 to 752 Pa). The range of experimental uncertainty is of similar magnitude to that for the vertical cavity. Thus, while $(Sh)_u$ for the case of isothermal moisture transfer ranged from 1.7 to 2.9, the $(Sh)_u$ for the case of combined transfer varied from 4.7 to 6.8. The Nusselt number, $(Nu)_u$, however, for the case of simultaneous heat and moisture being generally 5% greater than $(Nu)_u$ when the moisture gradient was absent. Since the experimental error in each case was about 12%, the difference is not significant. The practical implication from this observation is that, while a simultaneous temperature gradient significantly increases the transfer of moisture, the reverse case is not true.

A comparison between experimental and theoretical Sherwood numbers from this work is also presented in Fig. 12. The experimental Sherwood numbers are seen to agree with the theoretical line within the experimental limits of $\pm 20\%$. Again no other results from the literature were available for comparison with the data in Fig. 12. A best-fit line obtained by the least-squares technique

$$(Sh) = 0.144[Ra]^{0.272}_{T,C} \quad \text{S.D.} = 0.5 \qquad (17)$$

describes all the experimental Sherwood numbers in Fig. 12, again illustrating that the combined Rayleigh number is an appropriate parameter to characterize the respective driving forces for the various kinds of different buoyancy-generating mechanisms.

The Nusselt number correlation in Fig. 12 found by a least-squares technique is

$$(Nu) = 0.157[Ra]^{0.280}_{T,C} \quad \text{S.D.} = 0.5. \qquad (18)$$

The Nusselt number from equation (18) is about 8% higher than the experimental correlation of Hollands

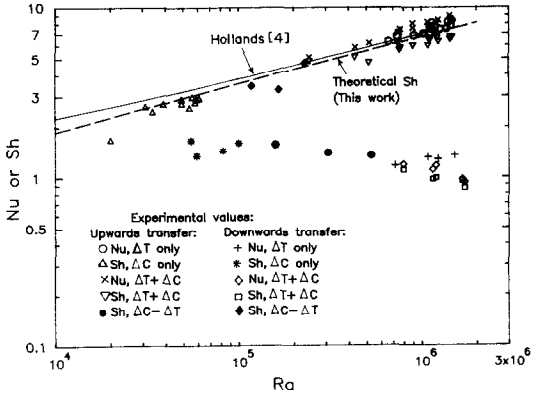

FIG. 12. Nusselt and Sherwood numbers for the horizontal cavity and the experimental correlation of Hollands [4].

[4]. Considering the experimental uncertainty for the Nusselt number is between 11 and 14%, the agreement is reasonable.

8.2.2. *A horizontal cavity with downwards transfer.* The Nusselt and Sherwood numbers for the downwards transfer cases are seen to agree with the expected value of 1.0 within experimental limits for the case of heat transfer and for aiding heat and moisture transfer. The Sherwood numbers for the isothermal case do not equal 1.0 within experimental limits. One possible reason for this discrepancy was the difficulty of maintaining an exact zero temperature gradient across the horizontal cavity. If there was a temperature difference of 0.5–0.8 K of the bottom surface over the top surface the convection current generated by the upwards temperature gradients would have been sufficient to give Sherwood numbers indicated in Fig. 12. The experimental uncertainty for the temperature difference for the downwards transfer case is about 0.36 K and hence the possibility of non-isothermal conditions in the cavity was high. However, the results for isothermal moisture transfer in the upwards direction were not affected in the same manner, which suggests that another reason was responsible for the rather high Sherwood number. Luikov and Berkotskii [33] have indicated that non-uniformity of boundary conditions over a flat surface can induce a convection current and hence increase the Sherwood number. The average deviation of the six surface temperature measurements from their mean value was about 5%; this measured variation might be enough to trigger surface convection. This phenomenon was not apparent for the case of simultaneous heat and moisture transfer because of the large stabilizing effect of the downwards temperature gradient which suppressed the surface convective current.

9. CONCLUDING REMARKS

The simultaneous transfer of heat and moisture in a rectangular cavity have been investigated experimentally and numerically. The cavity configurations used were those of a 'vertical cavity', 'horizontal cavity with upwards transfer' and 'horizontal cavity with downwards transfer'. Both aiding and opposing-gradients flow were investigated. The temperature difference used in the experiments ranged from 4 to 21 K (corresponding to Rayleigh numbers of 4×10^5–1.47×10^6). The vapour-pressure difference used in the experiments varied from 170 to 650 Pa (corresponding to the Rayleigh number range of 2.4×10^4–1.2×10^5). These conditions correspond to those expected to be found in practice in building cavities in New Zealand.

The rate of heat and moisture transfer in the vertical cavity and the horizontal cavity with upwards transfer was found to be five to nine times that of the horizontal cavity with downwards transfer. The corresponding Nusselt and Sherwood numbers for the horizontal cavity with downwards transfer was found

to attain the value of 1.0 within experimental limits. The presence of natural convection in the former two cases is responsible for the higher transfer rates. Further the Sherwood number for moisture transfer across an air-filled cavity will never attain the limit of 1.0 unless the presence of natural convection has been completely suppressed.

In the case of natural convection resulting from the range of temperature and moisture difference one would expect in practice, the dimensionless buoyancy driving force corresponding to the temperature difference $(Ra)_T$ was about ten times that generated by the moisture content difference $(Ra)_C$. Thus while the Sherwood number ranged from 1.7 to 2.9 in the absence of the simultaneous temperature gradient, it increased to 4.7 to 6.8 in the presence of it. The value of the Nusselt numbers, however, did not show any significant increase in the presence of the simultaneous moisture gradient.

The experimental Nusselt and Sherwood numbers reported in this paper agreed closely with the numerical results. This agreement verifies the use of the model in predicting the rate of heat and moisture transfer at any temperature and/or moisture gradient levels within the limits of the experimental data. The model may be extrapolated beyond the range of experimental limits, especially in the region of low temperature and moisture gradients where the conditions of the model are expected to hold but experimental validation was not possible due to the limitation of the apparatus.

REFERENCES

1. G. K. Batchelor, Heat transfer by free convection across a closed cavity between vertical boundaries at different temperature, *Q. Appl. Math.* **12**(3), 209–233 (1954).
2. E. R. G. Eckert and W. O. Carlson, Natural convection in an air layer enclosed between two vertical plates with difference temperatures, *Int. J. Heat Mass Transfer* **2**, 106–120 (1961).
3. Building Research Association of New Zealand, Programme of Work 1987–1988, Judgeford (1987).
4. K. G. T. Hollands, Multi-Prandtl number correlation equations for natural convection in layers and enclosures, *Int. J. Heat Mass Transfer* **27**, 466–468 (1984).
5. H. E. Robinson, L. A. Cosgrove and F. J. Powell, Thermal resistance of airspaces and fibrous insulations bounded by reflective surfaces, Building Materials and Structures, Report 151, National Bureau of Standards, U.S.A. (1957).
6. S. H. Yin, T. Y. Wung and K. Chen, Natural convection in an air layer enclosed within rectangular cavities, *Int. J. Heat Mass Transfer* **21**, 307–315 (1978).
7. M. J. Cunningham, A new analytical approach to the long term behaviour of moisture concentration in building cavities—Part 1: non-condensing cavity; Part 2: condensing cavity, *Bldg Envir.* **18**, 109–124 (1983).
8. M. J. Cunningham, Further analytical studies of building cavity moisture condensation, *Bldg Envir.* **19**, 21–29 (1984).
9. S. Ostrach, Natural convection in enclosures. In *Advances in Heat Transfer*, Vol. 18, pp. 161–227. Academic Press, New York (1972).
10. S. W. Churchill, Free convection in layers and enclosures. In *Heat Exchanger Design Handbook*, Vol. 2, *Fluid Mechanics and Heat Transfer*. Hemisphere, Washington, DC (1983).
11. T. K. Ross and A. A. Wragg, Electrochemical and mass transfer studies in annuli, *Electrochim. Acta* **10**, 1093–1106 (1965).
12. Y. Suzukawa and U. Narusawa, Structure of growing double-diffusive convection cells, *J. Heat Transfer* **104**, 248–254 (1982).
13. J. S. Turner, Double diffusive phenomena, *Ann. Rev. Fluid Mech.* **6**, 37 (1974).
14. D. M. Burch, A. G. Contreras and S. J. Treado, Use of low-moisture permeability insulation as an exterior retrofit system—a condensation study, *Trans. Am. Soc. Heat. Refrig. Air-Condit. Engrs* **85**(2), 547–562 (1979).
15. G. S. Dutt, Condensation in attics: are vapour barriers really the answer? *Energy Buildings* **2**, 251–258 (1979).
16. B. H. Vos and E. Tammes, Condensation in structures, Symp. on Moisture Problems in Buildings, The Hague, The Netherlands, Paper 2.3.5, 11 pp. (1975).
17. W. G. Mathers, A. J. Madden and E. L. Piret, Simultaneous heat and mass transfer in free convection, *Ind. Engng Chem.* **49**, 961–968 (1956).
18. E. V. Somers, Theoretical consideration of combined thermal and mass transfer from a vertical flat plate, *J. Appl. Mech.* **23**, 295–301 (1956).
19. J. A. Adams and P. W. McFadden, Simultaneous heat and mass transfer in free convection with opposing body forces, *A.I.Ch.E. Jl* **12**(4), 642–647 (1966).
20. J. A. Delefuw Denbouter, B. De Munnik and P. M. Heertjse, Simultaneous heat and mass transfer in laminar free convection from a vertical plate, *Chem. Engng Sci.* **23**, 1185–1190 (1968).
21. B. Gebhart and L. Pera, The nature of vertical natural convection flows resulting from the combined buoyancy effects of thermal and mass transfer, *Int. J. Heat Mass Transfer* **14**, 2025–2050 (1971).
22. R. H. Nilson and M. R. Baer, Double-diffusive counterbuoyant boundary layer in laminar natural convection, *Int. J. Heat Mass Transfer* **25**, 285–287 (1982).
23. A. Boura and B. Gebhart, The stability of a vertical flow which arises from combined buoyancy modes, *A.I.Ch.E. Jl* **22**(1), 94–102 (1976).
24. O. V. Trevisan and A. Bejan, Combined heat and mass transfer by natural convection in a vertical enclosure, *J. Heat Transfer* **109**, 104–112 (1987).
25. G. D. Mallinson and G. de Vahl Davis, The method of false transient for the solution of coupled elliptic equations, *J. Comput. Phys.* **12**, 435–461 (1973).
26. H. K. Wee, Heat and mass transfer in confined spaces, Ph.D. Thesis, University of Canterbury, Christchurch, New Zealand (1986).
27. S. Doss and K. Miller, Dynamic ADI method for elliptic equations, *SIAM J. Numer. Analysis* **106**, 837–856 (1979).
28. T. M. Phillips, Natural convection in an enclosed cavity, *J. Comput. Phys.* **54**, 365–381 (1984).
29. S. D. Probert and M. Dixon, Free convection within a vertical rectangular cavity subjected to large temperature differences, *Appl. Energy* **5**, 233–241 (1979).
30. ASTM C236-80, Standard test method for steady state thermal performance of building assemblies by means of a guarded hot box. *Annual Book of ASTM Standards*, Section 4, 04.06 (1984).
31. R. B. Keey and H. K. Wee, Free convective heat and mass transfer in rectangular building cavities, *Proc. CSIRO/DSIR Seminar on 'Convective Flows in Porous Media'* (Edited by R. A. Wooding and I. White), pp. 49–59. DSIR, Wellington, New Zealand (1985).
32. S. M. Elsherbiny, G. D. Raithby and K. G. T. Hollands, Heat transfer by natural convection across vertical and inclined air layers, *J. Heat Transfer* **104**, 96–102 (1982).
33. A. V. Luikov and B. M. Berkotskii, The onset of convection in cavities with variable wall temperatures, *Int. Chem. Engng* **9**(3), 414–417 (1969).

TRANSFERT DE CHALEUR ET D'HUMIDITE PAR CONVECTION NATURELLE DANS UNE CAVITE RECTANGULAIRE

Résumé—Le transfert simultané de chaleur et d'humidité par convection naturelle dans une cavité remplie d'air, de rapport de forme 7,0, est étudié numériquement et expérimentalement pour une cavité horizontale ou verticale. Les nombres de Prandtl et de Schmidt sont respectivement 0,7 et 0,6. Les équations aux différences finies sont résolues par la méthode implicite dynamique à directions alternées (DADI). On calcule les écoulements aidés et opposés pour des nombres de Grashof de chaleur et de concentration qui correspondent aux gradients réels de température et de concentration trouvés dans une cavité typique en Nouvelle Zélande ($2 \times 10^5 < Gr_T < 2 \times 10^6$ et $1 \times 10^4 < Gr_C < 2 \times 10^5$). La technique expérimentale utilise deux plaques plastiques poreuses comme parois de la cavité, permettant l'imposition des gradients simultanés de température et d'humidité. Les nombres expérimentaux de Nusselt et de Sherwood sont en bon accord avec les valeurs théoriques.

WÄRME- UND FEUCHTIGKEITSTRANSPORT DURCH NATÜRLICHE KONVEKTION IN EINEM RECHTECKIGEN HOHLRAUM

Zusammenfassung—Der gleichzeitige Transport von Wärme und Feuchtigkeit durch natürliche Konvektion in einem luftgefüllten Spalt mit einem Seitenverhältnis von 7,0 wird numerisch und experimentell sowohl für horizontale als auch für vertikale Orientierung des Spaltes untersucht. Die verwendete Prandtl-Zahl beträgt 0,7, die Schmidt-Zahl 0,6. Die Finite-Differenzen-Gleichungen werden mit dem dynamischen impliziten Verfahren der alternierenden Richtungen (DADI) gelöst. Sowohl gleich- als auch gegensinnige Strömungen werden für solche Bereiche der thermischen und konzentrationsbezogenen Grashof-Zahlen berechnet, welche mit typischen Temperatur- und Konzentrationsgradienten in Gebäuden übereinstimmen: ($2 \times 10^5 < Gr_T < 2 \times 10^6$ und $1 \times 10^4 < Gr_C < 2 \times 10^5$). Die Versuchsanordnung besteht aus zwei porösen Kunststoffplatten, mit denen gleichzeitig Feuchtigkeits- und Temperaturgradienten aufgebracht werden können. Berechnete und gemessene Nusselt- und Sherwood-Zahlen stimmen gut überein.

ЕСТЕСТВЕННОКОНВЕКТИВНЫЙ ТЕПЛО- И ВЛАГОПЕРЕНОС В ПРЯМОУГОЛЬНОЙ ПОЛОСТИ

Аннотация—Численно и экспериментально исследуется совместный естественноконвективный тепло- и влагоперенос в горизонтально и вертикально ориентированных заполненных воздухом полостях с отношением сторон 7,0. Используются значения чисел Прандтля и Шмидта, соответственно равные 0,7 и 0,6. Конечно-разностные уравнения решаются динамическим неявным методом переменных направлений. Рассчитываются совпадающие и встречные потоки в диапазонах значений теплового и концентрационного чисел Грасгофа, соответствующих реальным градиентам температуры и концентрации, характерных для внутренних объемов зданий, типичных для Новой Зеландии ($2 \times 10^5 < Gr_T < 2 \times 10^6$ и $1 \times 10^4 < Gr_C < 2 \times 10^5$). В эксперименте используются две пористые пластмассовые пластины в качестве стенок двух полостей, допускающих наложение совместных градиентов влаги и температуры. Найдено, что экспериментальные значения чисел Нуссельта и Шервуда хорошо согласуются с найденными теоретически.